Design and Performance Test of Pulse X-Ray Receiver Based on LYSO-SiPM for X-Ray Communication

Junxu Mu, Xiaobin Tang, Yunpeng Liu, Sheng Lai, Zhaopeng Feng, Wenxuan Chen, and Yiyang Wang

***Abstract*—X-ray communication (XCOM) is a type of wireless optical communication technology that uses modulated X-ray beam as the carrier of data transmission. As a core component of an XCOM system, the X-ray signal receiver determines the upper limit of the communication rate and the quality of communication. A pulse X-ray signal receiver based on an LYSO-SiPM detector and a field-programmable gate array signal processing module is designed to solve the problems of considerable background noise and weak signal strength in the actual XCOM process. The low bit error rate (BER) at the Mbps rate is realized first for XCOM. An XCOM performance test system is used to test the receiver's signal output characteristics and communication performance. The communication rate reaches 1.21 Mbps with BER less than 1.0×10^{-5}. The designed pulse X-ray signal receiver can effectively identify X-ray pulse under high bandwidth and weak signal receiving power.**

***Index Terms*—LYSO-SiPM, pulse X-ray signal receiver, signal processing module, X-ray communication.**

I. Introduction

X-RAY communication (XCOM) is a wireless optical communication technology using modulated X-ray beam as a data transmission carrier. In 2007, Dr. Keith Gendreau of the National Aeronautics and Space Administration (NASA) first proposed the concept of XCOM and conducted a communication verification experiment [1]. Compared with other communication modes, XCOM has the advantages of high theoretical communication rate [2], small diffraction limit, and good directivity; it is considered as the "next-generation aerospace communications technology" [3], [4]. The XCOM on-orbit experiment is scheduled to be demonstrated on the International Space Station by NASA [5] in the spring of 2019.

As a new communication mode, the performance of X-ray communication can't be comparable with state-of-the-art laser-based optical systems. However, as an effective supplementary extension of conventional communication methods, X-ray communication can exert its unique advantages to realize information transmission in some scenarios where traditional communication methods hardly operate. Considering that X-rays rapidly attenuate in the thick planetary atmosphere, X-ray communication is mainly used in environments where the atmosphere is very thin or absent, such as space, black barrier areas, and Martian dust storm environments [6]–[9]. Previous studies have shown that X-rays have strong penetrating capabilities and can achieve communication in those environments. Hang *et al.* [6] demonstrated that the stability of the communication link of XCOM in the dusty environment of Mars is better than that of the optical link. Li *et al.* [7], [8] showed the potential of XCOM for maintaining real-time communication during the spacecraft reentry into the Earth's atmosphere. Zhou *et al.* [9] showed that X-rays with energy over 30 keV have incredibly high penetration even in the high atmosphere of the Earth as well as the plasma sheath of reentry vehicles and obtained the data rate of 1 Mbps with the bit error rate (BER) of 10^{-6} at the transmitting power of 140 W. Therefore, XCOM has excellent potential in space communication and reentry communication.

XCOM uses intensity modulation direct detection to load and read the signal. The process is shown in Fig. 1. Similar to optical communication, the critical components of XCOM are modulated X-ray source, X-ray collimating/focusing optical system, and pulse X-ray signal receiver.

As a signal transmitter, the performance of modulated X-ray source directly determines the communication performance. At present, modulated X-ray sources mainly include light controlled modulated X-ray tube (LMXT) [10], field emission X-ray tube (FEXT) [11], and grid controlled modulated X-ray tube (GMXT) [12], which generate X-ray signals by adjusting light source or grid voltage. X-ray collimating/focusing optical system affects the transmission distance and power loss of X-ray signal. Wang *et al.* [13] designed a hard X-ray collimating/focusing optical system composed of nested confocal conical supermirrors, and the signal-to-noise ratio (SNR) reaches 71.8 dB at 100 km and 50.1 dB at 1000 km, respectively, when the transmitting power of X-ray is 100 W.

Manuscript received June 25, 2021; revised December 13, 2021 and February 8, 2022; accepted March 22, 2022. Date of publication March 25, 2022; date of current version July 2, 2022. This work was supported by the Aeronautical Science Fund under Grant 2018ZC52029.

Xiaobin Tang and Yunpeng Liu are with the Department of Nuclear Science and Technology, Nanjing University of Aeronautics and Astronautics, Nanjing 210016, China, and also with the Ministry of Industry and Information Technology, Key Laboratory of Nuclear Technology Application and Radiation Protection in Astronautics, Nanjing University of Aeronautics and Astronautics, Nanjing 210016, China (e-mail: tangxiaobin@nuaa.edu.cn; liuyp@nuaa.edu.cn).

Junxu Mu, Sheng Lai, Zhaopeng Feng, Wenxuan Chen, and Yiyang Wang are with the Department of Nuclear Science and Technology, Nanjing University of Aeronautics and Astronautics, Nanjing 210016, China (e-mail: mujunxu@nuaa.edu.cn; laisheng@nuaa.edu.cn; fengzhaopeng@nuaa.edu.cn; chengwenxuan@nuaa.edu.cn; yangyiwang@nuaa.edu.cn).

Color versions of one or more figures in this article are available at https://doi.org/10.1109/JLT.2022.3162344.

Digital Object Identifier 10.1109/JLT.2022.3162344

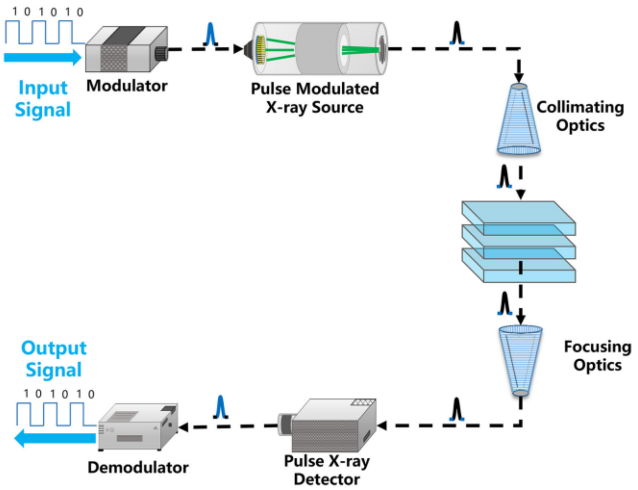

Fig. 1. XCOM system in the reentry blackout region.

TABLE I
THE PARAMETERS OF LYSO AND SIPM

	characteristics	parameter
	Thickness	5 mm
	Attenuation time	40 ns
	Light yield	28000 ph/MeV
	Emission peak	420 nm
	refractivity	1.81
SiPM	Spectral response range	250-950 nm
	Peak wavelength	420 nm
	PDE @ peak wavelength	35 %
	Gain	2.5×10^6
	Pixel size	50 μm × 50 μm
	Number of pixels	215296

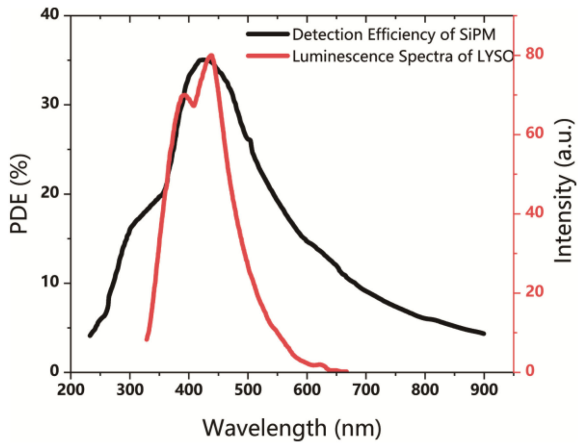

Fig. 2. The luminescence spectra curve of LYSO and the PDE curve of SiPM.

The pulse X-ray signal receiver determines the communication rate's quality and its upper limit. An X-ray signal receiver should have high bandwidth to support high-speed communication and high sensitivity to detect weak signals. In the current research on XCOM, the X-ray signal receivers used for signal reception are silicon drift detectors (SDD) [14], [15] and microchannel plate (MCP) detectors [16], [17]. These receivers have high detection efficiency for X-rays with 10–20 keV energy. However, the X-ray energy is usually as high as 30–100 keV in specific applications, such as communications in the black barrier area and the Martian dust environment. In this energy range, the detection efficiency of the above detectors is extremely low, and realizing communication is difficult. Except that, above detectors are mainly introduced from the X-ray energy spectrum measurement or pulsar measurement, and they are not specially designed for the XCOM system, resulting in the communication rate being limited to 100 kbps.

A pulse X-ray signal receiver based on the coupling of lutetium–yttrium oxyorthosilicate (LYSO) scintillator and silicon photomultiplier (SiPM) photodetector is proposed to meet the requirements of high detection efficiency and high bandwidth for the signal receiver in XCOM. The signal processing module of the receiver is designed based on a field-programmable grid array (FPGA). The communication bandwidth at Mbps level and BER on the order of 1.0×10^{-5} are realized.

II. DESIGN OF THE PULSE X-RAY SIGNAL RECEIVER

A. The Design Scheme of the Pulse X-Ray Detector

An LYSO scintillator and a JARY-TP3050-8×8C SiPM detection array are adopted to form the pulse X-ray detector. Their parameters are listed in Table I [18]. As shown in Fig. 2, the emission spectrum curve of LYSO [19] matches well with the quantum efficiency curve of SiPM. In order to further improve the collection efficiency of scintillation photons, the photons emission side of the LYSO crystal is coupled with SiPM by using optical grease, and the other sides of LYSO are deposited with a Teflon reflective layer and wrapped with insulating black tape. X-rays with less than 40 keV can ultimately deposit energy in a 5 mm thick LYSO scintillator. Based on the light yield and emission spectrum of the LYSO scintillator, its energy conversion efficiency is calculated to be 8.17%. According to the curves in Fig. 2, the energy conversion efficiency of SiPM is calculated to be 29.3%. Therefore, the overall energy conversion efficiency of the detector is 2.42%.

LYSO scintillator is inevitably doped with a small amount (2.6%) of ^{176}Lu isotope during preparation. ^{176}Lu decays by β emission accompanied with excited states of ^{176}Hf, and this process produces a background pulse signal, as shown in Fig. 3. LYSO spontaneously decays to 202 and 307 keV X-rays due to the radioactivity of ^{176}Lu [20]. These X-rays will increase the number of error symbols in the communication process and cause signal judgment and clock synchronization errors. Therefore, the subsequent signal processing module is further improved to solve this problem.

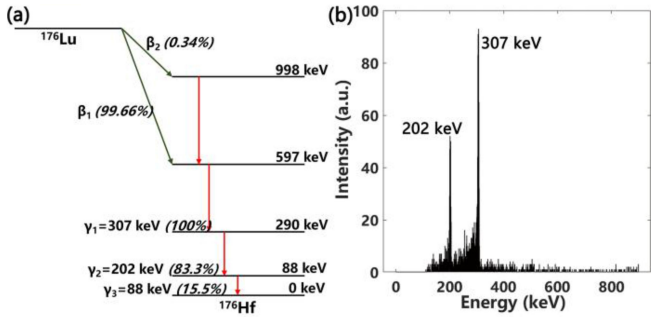

Fig. 3. (a) Simplified ^{176}Lu decay scheme and (b) ^{176}Lu energy spectrum.

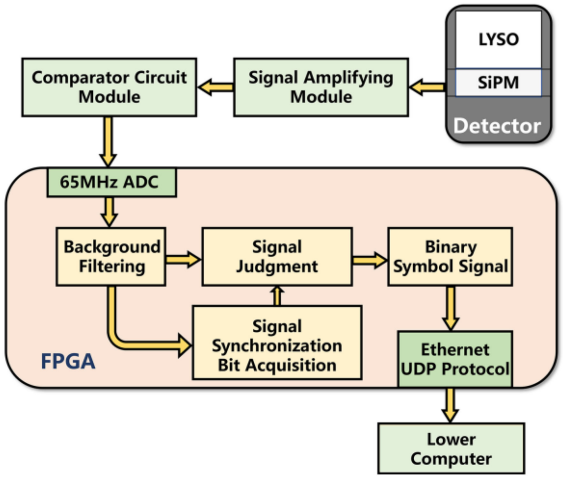

Fig. 4. Block diagram of pulsed X-ray receiver.

B. Hardware Design

The pulse X-ray receiver is successfully developed, as shown in Fig. 4. The signal processing circuit includes a signal amplifying module, a comparator circuit module, and an FPGA module.

The signal obtained by the detector is transmitted to the signal amplifying module through the coaxial RF connector. The signal boosting module is an amplifying circuit composed of voltage feedback operational amplifier chip AD8099. This module mainly performs amplitude amplification on the weak signal outputted by the detector.

The comparator circuit module performs pulse distinction and extraction on the amplified signal. This module is mainly composed of two high-speed comparison chips, LTC6752. The amplified signal enters the two-threshold distinguished circuits. The X-ray pulse signal threshold judgment and LYSO background threshold judgment are performed, and then two output pulse signals are obtained.

The FPGA module comprises Xilinx KINTEX-7 FPGA chip XC7K325TFFG900 and peripheral circuits. The two pulse signals generated by the comparator circuit module are sampled by two 65 MHz analog-to-digital converters (ADCs). The ADC's LVDS output is sent to the FPGA for digital pulse processing. Digital signal processing mainly includes background noise filtering, signal synchronization bit acquisition, signal judgment,

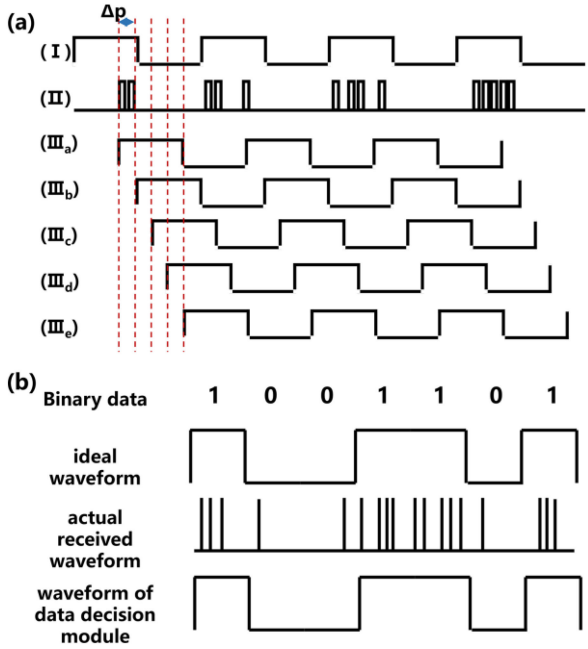

Fig. 5. Schematic of (a) signal synchronization bit acquisition and (b) signal judgment.

and other procedures. The binary symbol signal is obtained and transmitted to the lower computer for demodulation and decoding through the UDP network communication protocol.

C. Background Filtering

The function of this module is to filter out the background noise generated by the doped ^{176}Lu decays in LYSO scintillator. The signal enters the comparator circuit module and then into the threshold judgments of the X-ray pulse signal and the background noise. The pulse signals (1) and (2) with the same phase are obtained. The signal contains the X-ray carrier and the background noise, and signal (2) only has background noise. After the ADC samples the two signals, they enter the digital terminal and judge whether or not the high signal level (1) is retained under the high level in signal (2). At a specific time, when the channel (2) signal is high level and the channel (1) signal of the first two sampling points is low level, the duration of this channel (2) high-level pulse is determined as no X-ray carrier signal. Conversely, when the channel (2) signal is high level and the channel (1) signal of the first two sampling points at this time is high level, the duration of this channel (2) high-level pulse is determined as having an X-ray carrier signal.

D. Signal Synchronization Bit Acquisition

Fig. 5 shows the proposed recovery principle with the time slot synchronization clock. The transmitter signal uses the gated periodic square wave signal shown in Fig. 5(a) as the modulation signal. The receiving end generates several gated clock signals with the same period and different phases to recover the time slot synchronization clock at the receiving end. The phase difference between adjacent gated clock signals is Δp. During the high-level period of these clock signals, the counter is controlled to

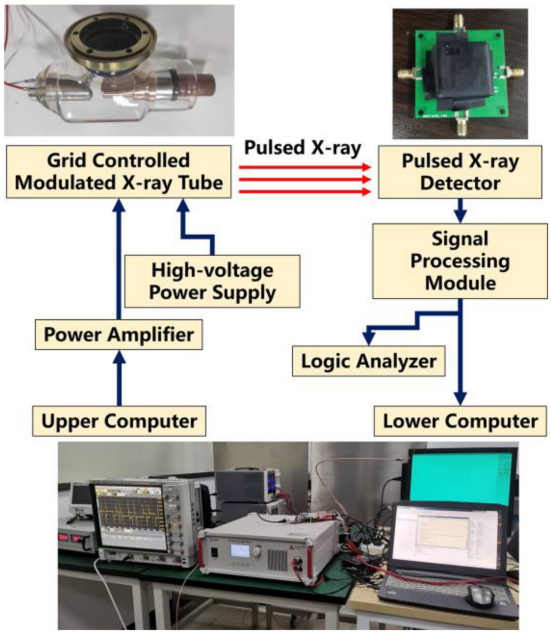

Fig. 6. Experimental setup of XCOM performance test system.

count the single-photon pulses outputted by the detector. The count value after multiple cycles is proportional to the width of the high-level overlap portion ($t1$, $t2$, $t3$ …). The difference in photon count values corresponding to several gating signals in several cycles may be unnoticeable due to the fluctuation of X-ray flux and detection efficiency. The maximum photon count value must come from the gating signal with the minimum phase difference from the time slot clock. Therefore, the receiver can select the gated periodic square wave signal corresponding to the maximum number of single-photon pulses as the clock signal to be recovered.

E. Signal Judgment

The proposed data judgment method is shown in Fig. 5(b). When the edge detection module detects the arrival of the rising and falling edges of the time slot synchronization clock signal, it outputs a flag signal into the counter module. Then the counter resets and recounts the number of single-photon pulses within the bit interval of the clock signal. Finally, the signal judgment module determines the bit information corresponding to the time slot by comparing the number of single-photon pulses in the synchronization clock signal of each time slot with the relative size of the set threshold. When the number of single-photon pulses in the time slot is greater than or equal to the threshold, the signal judgment module outputs a high level "1". Otherwise, the signal judgment module delays the one-time slot and outputs a low level "0".

III. Performance Test

An X-ray communication performance test system is built using the developed pulse X-ray receiver and the laboratory's existing grid controlled modulated X-ray tube, as shown in Fig. 6. The performance testing of the X-ray signal receiver

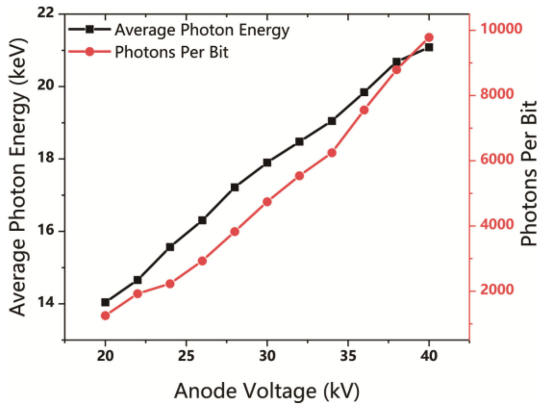

Fig. 7. Average photon energy and single bit photon number under different anode voltages.

is conducted in this XCOM system, which is also employed to verify the output signal characteristics of the receiver from the point of the communication performance.

The X-ray signal transmission process is carried out as follows. First, the upper computer generates a pseudo-random binary sequence signal and loads the signal to the power amplifier, converting the binary signals to −100V and 0V. Second, the voltage pulse generated by the power amplifier, called gird voltage, is applied on the grid of the GMXT to produce pulse electron beam, which hit an anode target driven by the anode voltage to emit pulse X-rays. Third, after passing through the air channel, the pulse X-ray signals reach the receiver. In the end, the binary signal is sent to the lower computer via Ethernet for offline demodulation and evaluation. During the process, the pseudo random binary sequence length is 2^{15}-1 and the estimate of transmitter on/off extension ratio of the system is 25.63 dB.

A. Power Calculation

In order to obtain the power-efficiency of the X-ray communication system, we utilize Monte Carlo toolkit Geant4 [21] to simulate the emission and transmission process of the X-ray signal and calculate the average energy and flux of the X-ray photons received by the signal receiver under different anode voltages, as shown in Fig. 7. The emission power of the X-ray tube is the product of the anode voltage and the anode current. In the experiment and simulation, the anode current is fixed at 1.35 A. Obviously, the emission power only depends on the anode voltage. The received power is the product of the average X-ray photons energy and the number of X-ray photons per bit. With the increase of anode voltage, both the number of single bit X-ray photons and the average photon energy increase. Under the anode voltage of 20–40 kV, the average photon energy increases from 14 keV to 22 keV, the single bit photon number changes in the range of 1250–9785, and the received light power is maintained at 2.8–30 μW.

B. Eye Diagram Test

For comparison, the signal characteristics of the developed pulse X-ray signal receiver and the conventional scheme are

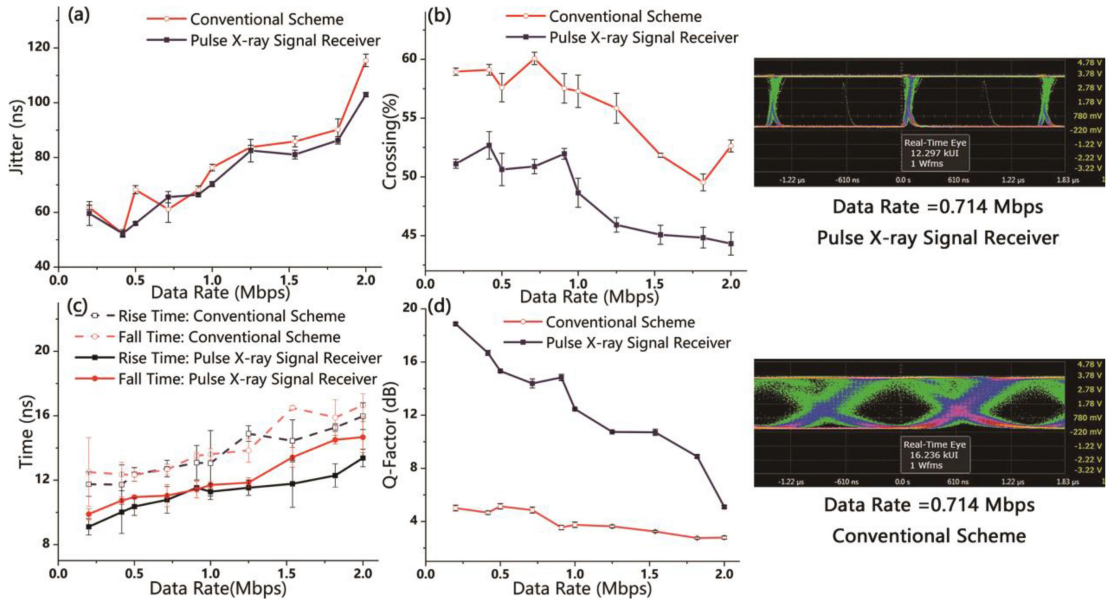

Fig. 8. Eye diagram characteristics at different data rates: (a) jitter, (b) crossing, (c) rise and fall times, (d) Q-factor.

tested simultaneously. In the conventional scheme, the signal generated by the detector is processed by the same amplifier module and comparator module, and enters the FPGA by ADC. But, the FPGA module does not include background noise filtering and signal synchronization bit acquisition, and it directly determines and outputs signals.

Under air channel conditions, a logic analyzer (RIGOL DS1104Z) is used to detect the changes in the eye diagram characteristics of the output signal of the X-ray receiver with the received power and data rat, respectively. The eye diagram characteristics studied in this paper include jitter, crossing, rise time, fall time, and Q-factor. Jitter and crossing reflect the degree of signal synchronization clock loss. The rise and fall times reflect the available bandwidth and the tolerable error rate ratio. The Q-factor comprehensively reflects the SNR of the signal.

Fig. 8 illustrates how the quality of the eye diagram changes with the data rate. In this experiment, the anode voltage of the X-ray tube is set to 30 kV, and the filament current is set to 1.35 A. As shown in Fig. 8(a), the jitter of the eye diagram gradually rises with the increase in the data rate, indicating that the timing noise of the signal continues to increase. This condition is possible because the intersymbol crosstalk gradually increases with the data rate. Fig.. 8(b) shows the change in the crossing with the data rate. When the data rate is less than 1 Mbps, the signal crossing of the X-ray signal receiver remains between 49% and 53%. The crossing gradually decreases after the data rate reaches above 1 Mbps. However, it remains above 44%, indicating that the signal strength of "1" decreases slightly and remains still within an acceptable range after the data rate reaches 1 Mbps or more. This X-ray signal receiver's eye jitter and crossing are significantly improved compared with the conventional scheme.

Fig. 8(c) illustrates how the rise and fall times change with the data rate. The rise and fall times of the proposed X-ray signal receiver are reduced by approximately 10% compared with the conventional scheme. With the increase in data rate, the rise and fall times of the eye diagram continue to increase, but they are less than 18 ns, thereby meeting the XCOM rate requirement. Similar to the experimental results discussed above, the Q-factor of the eye diagram gradually decreases as the data rate increases in Fig. 8(d). This phenomenon is mainly because the high data rate reduces the intensity of the unit pulse signal. The Q-factor of the proposed X-ray signal receiver is significantly better than the conventional scheme. The Q-factor of the eye diagram for the receiver is still higher than 8 dB when the communication rate is lower than 1.8 Mbps. While, the Q-factor of the conventional scheme is always lower than 6 dB in tests at all speeds due to the poor SNR.

The change in eye diagram quality with the received power of the X-ray tube is shown in Fig. 9. In this experiment, the data rate is 0.714 Mbps, and the filament current is 1.35 A. When the received power is below 10 μW, the transmitter's signal strength is feeble, making the jitter and crossing poor, as shown in Figs. 9(a) and (b). With the increase in received power, the signal crossing of the proposed X-ray signal receiver gradually increases and remains between 50% and 53% at 10 μW or more. The jitter of the eye diagram gradually decreases. The crossing and jitter of the proposed receiver are significantly better than the conventional scheme.

Fig. 9(c) illustrates the change in rise and fall times with the received power. Compared with the conventional scheme, the rise and fall times of the proposed X-ray signal receiver are slightly reduced. With the increasing in received power, the rise and fall times of the eye diagram decrease. The rise and fall times are less than 20 ns when the received power is higher than 10 μW. As shown in Fig. 9(d), the Q-factor of the conventional eye diagram increases with the received power; however, it is always lower than 6 dB. The signal eye diagram Q-factor of the proposed X-ray signal receiver illustrates rising and then falling with the received power. When the received power is low, the signal strength is weak. Thus, the signal quality gradually increases with the increase in received power. However, over 10 μW, the pulse height of the signal is similar to the pulse height of

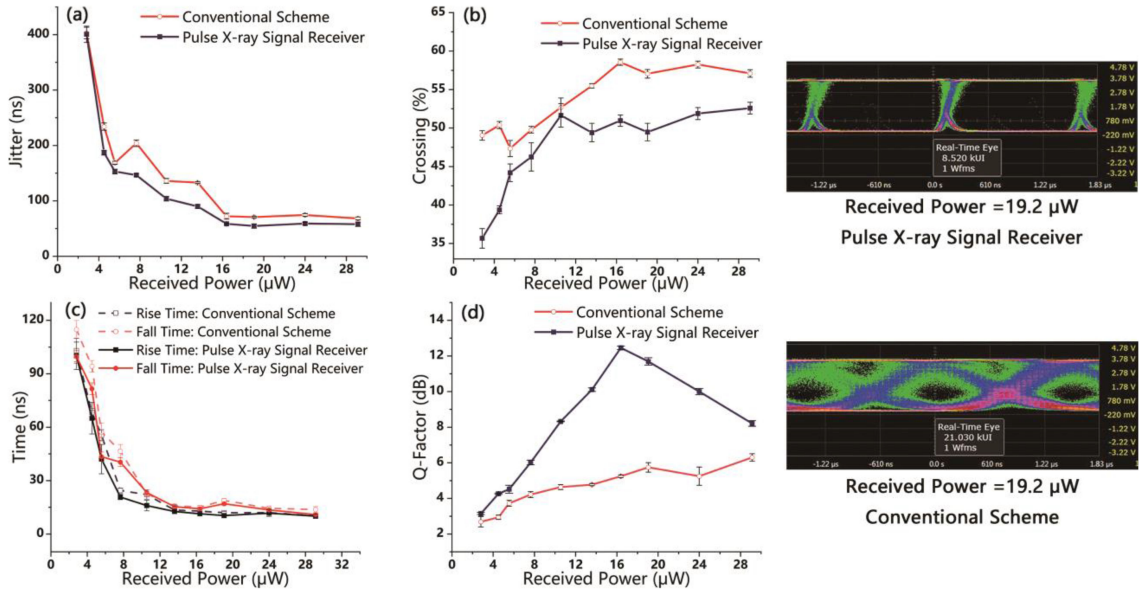

Fig. 9. Eye diagram characteristics at different received powers: (a) jitter, (b) crossing, (c) rise and fall times, (d) Q-factor.

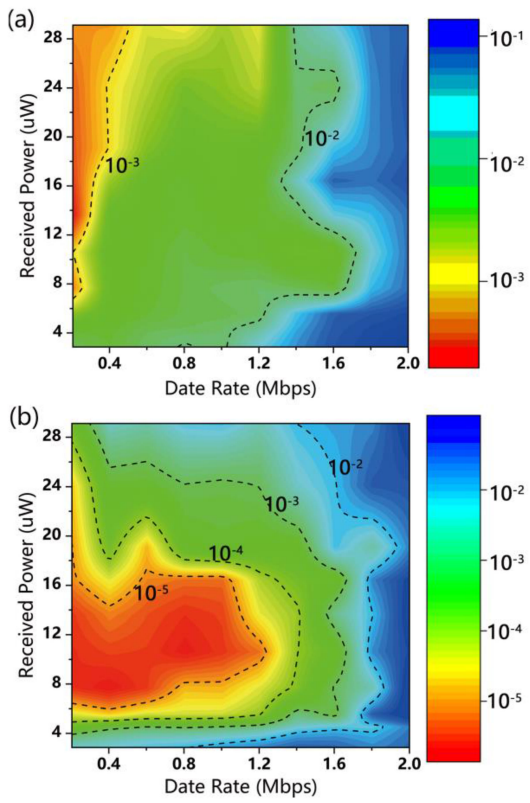

Fig. 10. BER versus different date rates and received power: (a) conventional scheme, (b) pulse X-ray signal receiver Communication performance test.

the background noise generated by the scintillator itself, causing the "background filtering module" to filter part of the valid signal and reducing the Q-factor.

Fig. 10 compares the communication performance of the XCOM system. Under the same conditions, the error rate of the proposed X-ray signal receiver system is significantly reduced by one to two orders of magnitude compared with the conventional scheme. When the data rate is below 1.21 Mbps, and the received power is between 6-16 μW, the XCOM system's error rate is lower than 1.0×10^{-5}. This result proves that the proposed pulse X-ray signal receiver can filter high-intensity background noise and detect low-power signals.

As shown in Fig. 10(b), the system's BER gradually decreases with the increase in the data rate under a particular signal strength. The unit pulse time slot decreases with the increase in the data rate. The width of the background noise generated by the scintillator itself is a fixed value. Thus, its proportion gradually increases, thereby increasing the BER.

With the increase in received power, the X-ray signal receiver system's error rate gradually decreases firstly, reaches the lowest point at approximately 10 μW, and then slowly rises. This result is consistent with the relationship between the Q-factor and the received power in Fig. 9(d). This phenomenon is because the pulse height of the signal is similar to the pulse height of the background noise generated by the scintillator itself when the received power is higher than 10 μW. Thus, the background filtering module filters part of the correct signal, increasing the BER. This problem is caused by the amplitude limitation of the signal amplification module. This part will be improved in future work to solve this problem.

C. Sensitivity Analysis

The relationship between received power and bit error rate at different data rates is shown in Fig. 11. It can be seen that under different bit error rate conditions, the minimum received power maintains an upward trend as the data rate increases. If the system's sensitivity is defined as the minimum received power of the receiver when the BER reaches 10^{-5}, the sensitivity remains at -22.2 to -19.8 dBm at a data rate of 0.2–1.2 Mbit/s, increasing slowly with increasing speed. When the data rate is much higher

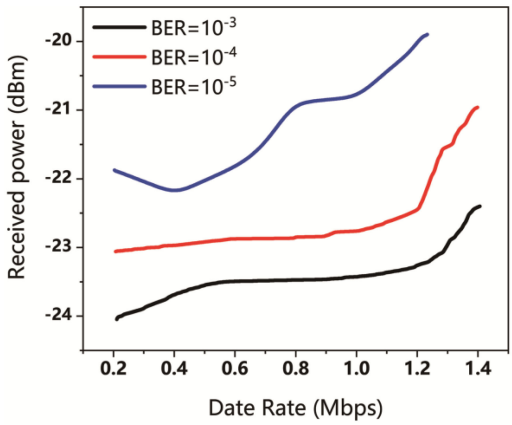

Fig. 11. The relationship between received power and BER under different data rates.

than 1.2 Mbit/s, the bit time is close to the output pulse width of the receiver so that the required received power increases rapidly at the same BER.

The receiving power is really high in XCOM compared with the optical communication. The main reason is the low energy conversion efficiency of the LYSO scintillator to the X-ray signal. Although the LYSO scintillator can effectively detect X-rays with energy greater than 30 keV, its energy conversion efficiency is only 8.17%, resulting in a power waste of -10.8 dB. In the following work, we will try to use scintillators with better light yield or try to use new semiconductor materials such as CZT detectors to directly detect X-rays to improve the receiver sensitivity. In the following work, scintillators with better optical yield or new semiconductor materials will be tried to detect X-ray pulse signals to enhance the receiver's sensitivity. In addition, the considerable noise power of the receiver is also one of the reasons for the unsatisfactory sensitivity. In the future work, we will further improve the performance of the receiver by improving the noise filtering module.

The experimental results prove that the low BER ($<10^{-5}$) X-ray communication at Mbps rate is realized for the first time using the X-ray signal receiver designed in this paper. The existing signal receivers, SDD [15] and MCP [17], used for X-ray communication, can only achieve X-ray communication at a 25 kbps rate under the same BER. This comparison result proves the superiority of the proposed LYSO-SiPM pulsed X-ray signal receiver.

IV. Conclusion

A pulse X-ray signal receiver, including an LYSO-SiPM detector and signal processing module, is designed for X-ray communication. The signal processing module of the receiver is designed based on FPGA. This module realizes background filtering, signal synchronization bit acquisition, signal judgment, and other programs. It also solves the problem of poor communication performance caused by considerable background noise and weak signal strength in the actual communication process. Experimental results verify the system's signal characteristics and BER performance at different data rates and received powers. The Q-factor of the eye diagram of the pulse X-ray signal receiver is always higher than 6 dB. When the data rate is less than 1.21 Mbps and the received power is between 6-16 μW, the BER of the pulse X-ray signal receiver is less than 1.0×10^{-5}. The proposed solution achieves the filtering of high-intensity background noise and the detection of low-power signals. The experimental results prove the feasibility and superiority of the proposed LYSO-SiPM pulsed X-ray signal receiver.

References

[1] K. Gendreau, "Next-Generation communications: 'Demonstrating the world's first X-Ray communication system'," Rep. no. FS-2007-10-103-GSFC (TT#7), NASA, Washington, DC, USA, 2007.
[2] G. Porter, "See straight through data center bandwidth limitations with X-rays," 2013.
[3] B. Zhao *et al.*, "Next generation of space wireless communication technology based on X-ray," *Acta Photon. Sinica*, vol. 42, no. 7, pp. 801–804, 2013.
[4] P. J. Winzer, "Would scaling to extreme ultraviolet or soft X-ray communications resolve the capacity crunch?," *J. Lightw. Technol.*, vol. 36, no. 24, pp. 5786–5793, Dec. 2018, doi: 10.1109/JLT.2018.2877575.
[5] L. Keesey, "NASA set to demonstrate X-ray communications in space," NASA's Goddard Space Flight Center, Feb. 19, 2019. [Online]. Available: https://phys.org/news/2019-02-nasa-X-ray-space.html
[6] S. Hang *et al.*, "Potential application of X-ray communication in Martian dust storm," *Acta Astronautica*, vol. 166, pp. 277–289, 2020.
[7] H. Li *et al.*, "Potential application of X-ray communication through a plasma sheath encountered during spacecraft reentry into earth's atmosphere," *J. Appl. Phys.*, vol. 121, no. 12, 2017, Art. no. 123101.
[8] Y. Liu *et al.*, "Transmission properties and physical mechanisms of X-ray communication for blackout mitigation during spacecraft reentry," *Phys. Plasmas*, vol. 24, no. 11, 2017, Art. no. 113507.
[9] W. Zhou *et al.*, "Power budget and performance analysis of X-ray communication during the Earth re-entry of spacecraft," *Optik*, vol. 199, 2019, Art. no. 163521.
[10] H. Xuan *et al.*, "Light-controlled pulsed X-ray tube with photocathode," *Chin. Phys. B*, vol. 30, 2021, Art. no. 118502.
[11] S. Lai *et al.*, "X-ray high frequency pulse emission characteristic and application of CNT cold cathode X-ray source cathode X-ray source," *Nanotechnology*, vol. 33, 2021, Art. no. 075201.
[12] G. Davidoff *et al.*, "A modulated X-ray source controller for the in-flight calibration of X-Ray astronomy payloads," 2010.
[13] Y. Wang *et al.*, "Collimating/focusing optical system designed for hard X-ray communication," *Nucl. Instrum. Methods Phys. Res. Sect. A: Accelerators, Spectrometers, Detectors Assoc. Equip.*, vol. 1016, 2021, Art. no. 165776.
[14] G. Prigozhin *et al.*, "NICER instrument detector subsystem: Description and performance," in *Proc. Space Telescopes Instrum.: Ultraviolet Gamma Ray*, 2016, Art. no. 99051I.
[15] Y. Liu *et al.*, "X-ray communication experiment using photocathode X-ray tube," in *Proc. 7th Symp. Novel Photoelectron. Detection Technol. Appl.*, 2021, Art. no. 117638U.
[16] Q. Zhou *et al.*, "The test and analysis on pulse signal detection abilities of the X-ray detector MCP for pulsar navigation," in *Proc. China Satell. Navigation Conf.*, 2017, pp. 637–647.
[17] Y. Li *et al.*, "Bit error rate analysis of the spatial X-ray communication system," *Infrared Laser Eng.*, vol. 47, 2018, Art. no. 6.
[18] "TP3050 SiPM array product data sheet," [Online]. Available: http://www.joinbon.com/Uploads/file/20200713/20200713141027_68938.pdf
[19] R. Mao, L. Zhang, and R.-Y. Zhu, "Quality of a 28 cm long LYSO crystal and progress on optical and scintillation properties," *IEEE Trans. Nucl. Sci.*, vol. 59, no. 5, pp. 2224–2228, Oct. 2012.
[20] H. Alva-Sánchez *et al.*, "Understanding the intrinsic radioactivity energy spectrum from 176 Lu in LYSO/LSO scintillation crystals," *Sci. Rep.*, vol. 8, no. 1, pp. 1–7, 2018.
[21] "Geant4: A simulation toolkit," [Online]. Available: https://geant4.web.cern.ch/